BVRI Photometry of SN 2013ej in M74

Michael W. Richmond
School of Physics and Astronomy, Rochester Institute of Technology, 84 Lomb Memorial Drive, Rochester, NY 14623; mwrsps@rit.edu

Received May 19, 2014; revised June 24, 2014; accepted June 25, 2014

Abstract I present BVRI photometry of the type IIP supernova 2013ej in M74 from 1 to 179 days after its discovery. These photometric measurements and spectroscopic data from the literature are combined via the expanding photosphere method to estimate the distance to the event, which is consistent with that derived by other methods. After correcting for extinction and adopting a distance modulus of $(m - M) = 29.80$ mag. to M74, I derive absolute magnitudes $M_B = -17.36$, $M_V = -17.47$, $M_R = -17.64$, and $M_I = -17.71$. The differences between visual measurements and CCD *V*-band measurements of SN 2013ej are similar to those determined for type Ia supernovae and ordinary stars.

1. Introduction

On UT 2013 July 25.45, the Lick Observatory Supernova Search (LOSS) detected a new point source in the nearby galaxy M74 (NGC 628); when the object appeared again and brighter the next night, LOSS alerted other astronomers to the presence of this new object. Within days, spectroscopy revealed it to be a young type II supernova, designated SN 2013ej (Kim *et al.* 2013). Because its host is so nearby (less than 10 Mpc; see section 5) and so well studied, and because the event was caught within a few days of the explosion, SN 2013ej provides a fine opportunity for us to study the properties of a massive star before and after it undergoes core collapse.

I present here photometry of SN 2013ej in the *BVRI* passbands obtained at the RIT Observatory, starting one day after the announcement and continuing for a span of 179 days. Section 2 describes the observational procedures, the reduction of the raw images, and the methods used to extract instrumental magnitudes. In section 3, I explain how the instrumental quantities were transformed to the standard Johnson-Cousins magnitude scale. I illustrate the light curves and color curves of SN 2013ej in section 4 and comment briefly on their properties. In section 5, I discuss extinction along the line of sight to this event. In section 6, I discuss attempts to measure the distance to M74, and use the Expanding Photosphere Method (EPM) to perform my own estimate; I adopt a distance and convert the apparent magnitudes at peak to absolute magnitudes. Visual measurements of this event collected by the American Association of Variable Star Observers (AAVSO 2013) are compared to CCD *V*-band measurements in section 7. I summarize the results of this study in section 8.

2. Observations

This paper contains measurements made at the RIT Observatory, near Rochester, New York. The RIT Observatory is located on the campus of the Rochester Institute of Technology, at longitude 77:39:53 West, latitude +43:04:33 North, and an elevation of 168 meters above sea level. The eastern horizon is bright and dominated by a large pine tree. Measurements during the first two weeks, and particularly on the very first night, were taken at low airmass and not far from the tree's branches. I used a Meade LX200 f/10 30-cm telescope and SBIG ST-8E camera, which features a Kodak KAF1600 CCD chip and astronomical filters made to the Bessell (1990) prescription; with 3 × 3 binning, the plate scale is 1.85" per pixel. To measure SN 2013ej, I took a series of 30-second exposures through each filter, using the autoguider if possible; the only guide star was very faint in the *B*-band, so most of those images were unguided. The number of exposures per filter ranged from ten, at early times, to fifteen or thirty at late times. I typically discarded a few images in each series due to trailing. I acquired dark and flatfield images each night, except for UT Dec 17; the images from that night were reduced using dome flats taken the following evening. In most cases, I chose to use dome flats over twilight sky flatfield images.

I combined ten dark images each night to create a master dark frame, and ten flatfield images in each filter to create a master flatfield frame. After applying the master dark and flatfield images in the usual manner, I examined each cleaned target image by eye. I discarded trailed and blurry images and measured the Full Width at Half Maximum (FWHM) of those remaining. The XVista (Treffers and Richmond 1989) routines STARS and PHOT were used to find stars and to extract their instrumental magnitudes, respectively, using a synthetic aperture with radius of 4 pixels (= 7.4"), slightly larger than the FWHM (which was typically 4" to 5").

As Figure 1 shows, SN 2013ej lies in the outskirts of one of the spiral arms of M74. How much light from other objects in the area falls into the aperture used to measure the supernova? I examined high-resolution HST images of this region, using ACS WFC data in the F435W, F555W, and F814W filters originally taken as part of proposal GO-10402 (PI: Chandar). See Fraser *et al.* (2014) for a detailed analysis of the progenitor's light in these images. Within a circle of radius 7.4" centered on the SN's position are ten or so point sources of roughly equal brightness, with magnitudes of roughly $B \sim 25$, $I \sim 23$. The combined light of these sources is too small to make a significant addition to the light of the SN itself. However, a considerably brighter source lies at R.A. $01^h\ 36^m\ 48.55^s$, Dec. +15º 45' 26.5", a distance of 7.7" to the southeast of SN 2013ej. Comparing it to the progenitor in the HST images, I measure magnitudes of $B = 22.64$, $V = 21.15$, $I = 18.10$. The *I*-band value agrees well with an entry in the *USNO B1.0 Catalog* (Monet *et al.* 2003). Since this star lies at the edge of

the synthetic aperture used to measure the SN, some of its light was attributed to the SN in my measurements. In the *B* and *V* images, SN 2013ej was at least 3.9 magnitudes brighter than this star at all times, and so the contaminating flux was at most a few percent. In the *R* and *I* images, on the other hand, this star's light may have been important at late times. In the last *I*-band measurement, for example, roughly one-sixth of the measured light may have come from this star. Since the exact amount of contamination depends on details of the seeing and shape of the point-spread function on each night, I have made no correction for this effect; but the late-time measurements reported here are slightly brighter than they ought to be, especially in the red passbands.

Between July and early September, 2013, I measured instrumental magnitudes from each exposure and applied inhomogeneous ensemble photometry (Honeycutt 1992) to determine a mean value in each passband. Starting on UT Sep 11, 2013, in order to improve the signal-to-noise ratio, I combined the good images for each passband using a pixel-by-pixel median procedure to yield a single image with lower noise levels. I then extracted instrumental magnitudes from this image in the manner described above. In order to verify that this change in procedure did not cause any systematic shift in the results, I also measured magnitudes from the individual exposures at these late times, reduced them using ensemble photometry, and compared the results to those measured from the median-combined images. As Figure 2 shows, there were no significant systematic differences.

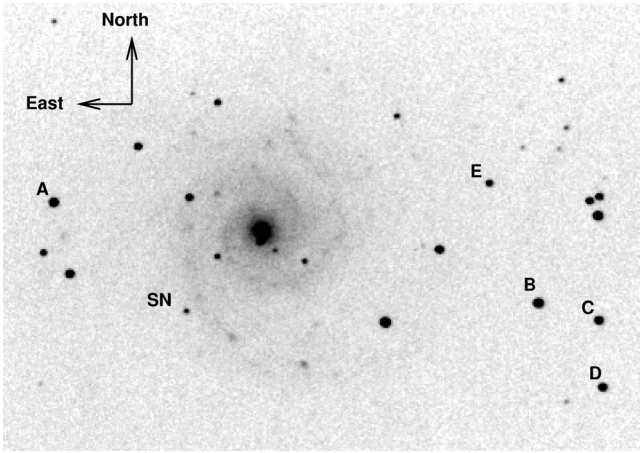

Figure 1. An R-band image of M74 from RIT, 15 × 30 seconds exposure time, showing stars used to calibrate measurements of SN 2013ej. North is up, East to the left. The field of view is roughly 12 by 9 arcminutes.

Table 1. Photometry of comparison stars.

Star	*R.A. (J2000)* *h m s*	*Dec. (J2000)* *° ′ ″*	*B*	*V*	*R*	*I*
A	01 36 58.63	+15 47 46.7	13.012 ± 0.019	12.510 ± 0.019	12.154 ± 0.019	11.834 ± 0.019
B	01 36 19.55	+15 45 22.4	13.848 ± 0.026	13.065 ± 0.022	12.622 ± 0.025	12.152 ± 0.027
C	01 36 14.64	+15 44 58.6	14.338 ± 0.029	13.692 ± 0.024	13.329 ± 0.029	12.964 ± 0.030
D	01 36 14.60	+15 43 39.5	14.832 ± 0.027	13.912 ± 0.023	13.416 ± 0.026	12.939 ± 0.030
E	01 36 23.06	+15 47 45.4	15.192 ± 0.034	14.613 ± 0.027	14.275 ± 0.034	13.915 ± 0.036

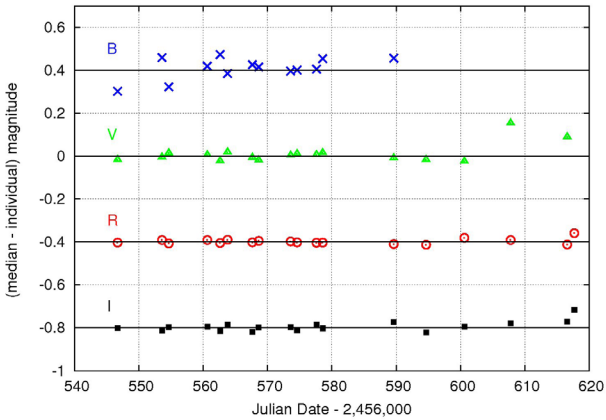

Figure 2. Difference between instrumental magnitudes extracted from median-combined images and from individual images at RIT. The values have been shifted for clarity by 0.4, 0.0, –0.4, –0.8 magnitude in B, V, R, I, respectively.

3. Photometric calibration

In order to transform the instrumental measurements into magnitudes in the standard Johnson-Cousins BVRI system, I used a set of local comparison stars, supplied by the AAVSO in their chart 12459CA. These reference stars are listed in Table 1, and Figure 1 shows their location.

In order to correct for differences between the RIT equipment and the Johnson-Cousins system, I observed the standard fields PG1633+009 and PG2213-006 (Landolt 1992) on several nights and compared the instrumental magnitudes to catalog values. Linear fits to the differences as a function of color yielded the following relationships:

$$B = b + (0.231 \pm 0.012) \times (b - v) + Z_B \quad (1)$$

$$V = v - (0.079 \pm 0.017) \times (v - r) + Z_V \quad (2)$$

$$R = r - (0.087 \pm 0.021) \times (r - i) + Z_R \quad (3)$$

$$I = i - (0.018 \pm 0.040) \times (r - i) + Z_I \quad (4)$$

In the equations above, lower-case symbols represent instrumental magnitudes, upper-case symbols Johnson-Cousins magnitudes, and Z the zeropoint in each band. Stars A, B, C, D, and E were used to set the zeropoint for each image. Table 2 lists the calibrated measurements of SN 2013ej made at RIT. The first column shows the mean Julian Date of all the exposures taken during each night. In most cases, the span between the first and last exposures was less than 0.04 day, but on a few nights, clouds interrupted the sequence of observations. Contact the author for a dataset providing the Julian Date of each measurement individually.

Table2.PhotometryofSN2013ej.

JD–2456500	*B*	*V*	*R*	*I*	*comments*
0.71	12.945 ± 0.059	12.999 ± 0.025	12.972 ± 0.060	12.967 ± 0.056	high airmass
3.80	12.714 ± 0.035	12.647 ± 0.012	12.566 ± 0.021	12.537 ± 0.025	cirrus
4.73	12.693 ± 0.020	12.615 ± 0.019	12.509 ± 0.027	12.446 ± 0.058	cirrus
6.81	12.624 ± 0.047	12.524 ± 0.021	12.404 ± 0.018	12.373 ± 0.025	
8.75	12.668 ± 0.048	12.522 ± 0.014	12.370 ± 0.030	12.275 ± 0.037	clouds
9.73	12.700 ± 0.056	12.513 ± 0.042	12.350 ± 0.034	12.318 ± 0.041	
10.83	12.715 ± 0.028	12.553 ± 0.032	12.321 ± 0.043	12.291 ± 0.052	clouds
14.69	12.964 ± 0.056	12.527 ± 0.075	12.297 ± 0.051	12.239 ± 0.034	clouds
15.70	12.973 ± 0.036	12.548 ± 0.013	12.303 ± 0.015	12.219 ± 0.030	
19.70	13.239 ± 0.032	12.586 ± 0.026	12.310 ± 0.028	12.176 ± 0.035	
20.68	13.351 ± 0.086	12.601 ± 0.028	12.309 ± 0.043	12.149 ± 0.042	cirrus
21.70	13.421 ± 0.084	12.651 ± 0.032	12.339 ± 0.031	12.177 ± 0.043	
24.69	13.564 ± 0.094	12.748 ± 0.039	12.378 ± 0.028	12.237 ± 0.051	
25.69	13.734 ± 0.137	12.787 ± 0.058	12.429 ± 0.026	12.211 ± 0.034	nearby moon
28.70	13.831 ± 0.056	12.864 ± 0.038	12.470 ± 0.025	12.255 ± 0.036	
29.66	13.939 ± 0.090	12.904 ± 0.027	12.507 ± 0.030	12.290 ± 0.038	
33.68	14.109 ± 0.085	13.026 ± 0.045	12.574 ± 0.023	12.340 ± 0.028	
38.62	14.346 ± 0.140	13.142 ± 0.034	12.677 ± 0.021	12.403 ± 0.062	clouds
39.79	14.406 ± 0.039	13.164 ± 0.026	12.686 ± 0.019	12.446 ± 0.030	
41.75	14.442 ± 0.052	13.228 ± 0.024	12.734 ± 0.020	12.491 ± 0.045	clouds
44.62	14.495 ± 0.096	13.291 ± 0.037	12.765 ± 0.024	12.514 ± 0.035	high airmass
46.68	14.642 ± 0.094	13.302 ± 0.028	12.824 ± 0.027	12.542 ± 0.051	
53.57	14.747 ± 0.084	13.438 ± 0.031	12.902 ± 0.026	12.587 ± 0.029	nearby moon

Table continued on next page

Table2.PhotometryofSN2013ej, cont.

JD–2456500	*B*	*V*	*R*	*I*	*comments*
54.63	14.889 ± 0.048	13.450 ± 0.039	12.909 ± 0.016	12.627 ± 0.021	nearby moon
60.62	14.932 ± 0.055	13.538 ± 0.055	13.007 ± 0.018	12.699 ± 0.026	
62.62	14.993 ± 0.056	13.570 ± 0.041	13.006 ± 0.016	12.691 ± 0.026	clouds
63.77	14.955 ± 0.072	13.618 ± 0.025	13.037 ± 0.020	12.746 ± 0.025	
67.62	15.082 ± 0.070	13.634 ± 0.041	13.080 ± 0.020	12.759 ± 0.022	
68.62	15.119 ± 0.060	13.650 ± 0.046	13.110 ± 0.022	12.780 ± 0.030	hazy
73.59	15.285 ± 0.067	13.733 ± 0.031	13.172 ± 0.037	12.864 ± 0.031	
74.59	15.234 ± 0.068	13.771 ± 0.040	13.191 ± 0.021	12.900 ± 0.024	
77.60	15.321 ± 0.065	13.858 ± 0.038	13.230 ± 0.022	12.947 ± 0.032	clouds
78.56	15.357 ± 0.093	13.868 ± 0.043	13.280 ± 0.021	12.967 ± 0.027	
89.58	15.807 ± 0.077	14.211 ± 0.034	13.599 ± 0.030	13.300 ± 0.037	clouds
94.65	—	14.299 ± 0.043	13.913 ± 0.024	13.602 ± 0.039	
96.62	16.412 ± 0.149	14.907 ± 0.051	14.174 ± 0.035	13.811 ± 0.050	
100.58	17.166 ± 0.161	15.776 ± 0.079	14.954 ± 0.047	14.631 ± 0.066	clouds
107.79	18.193 ± 0.311	16.612 ± 0.137	15.388 ± 0.062	15.044 ± 0.082	
110.64	—	16.309 ± 0.133	15.378 ± 0.082	15.100 ± 0.119	clouds
113.64	—	16.572 ± 0.160	15.584 ± 0.083	15.219 ± 0.110	clouds
116.59	—	16.478 ± 0.123	15.501 ± 0.064	15.180 ± 0.090	
117.71	—	16.444 ± 0.135	15.497 ± 0.078	15.132 ± 0.107	cirrus
130.48	—	16.889 ± 0.247	15.763 ± 0.110	15.674 ± 0.175	cirrus
143.52	—	17.235 ± 0.237	16.001 ± 0.100	15.561 ± 0.149	clouds
155.49	—	17.089 ± 0.217	16.144 ± 0.109	16.132 ± 0.196	

The uncertainties listed in Table 2 incorporate the uncertainties in instrumental magnitudes and in the offset used to shift the instrumental values to the standard scale, added in quadrature. As a check on their size, I chose a region of the light curve, 40 < JD – 2456500 < 80, in which the magnitude appeared to be a linear function of time. I fit a straight line to the measurements in each passband, weighting each point based on its uncertainty; the results are shown in Table 3. The reduced χ^2 values are all less than 1.0, which suggests that the tabulated uncertainties slightly overestimate the random scatter from one measurement to the next.

4. Light curves

The light curves in each passband, uncorrected for any extinction, are shown in Figure 3. SN 2013ej is clearly a type IIP event, defined by a period of roughly 60 days during which the apparent brightness decreases very slowly. The plateau phase ends at Julian Date ~2456590, after which there is a sharp drop lasting a week or so. The light curve then decreases at a moderate pace for another month, to the end of the observations.

Table 3. Linear fit to light curves 40 < JD – 2456500 < 80.

Passband	*Slope (mag./day)*	*Reduced χ^2*
B	0.0238 ± 0.0012	0.6
V	0.0167 ± 0.0004	0.3
R	0.0141 ± 0.0003	0.5
I	0.0131 ± 0.0006	0.8

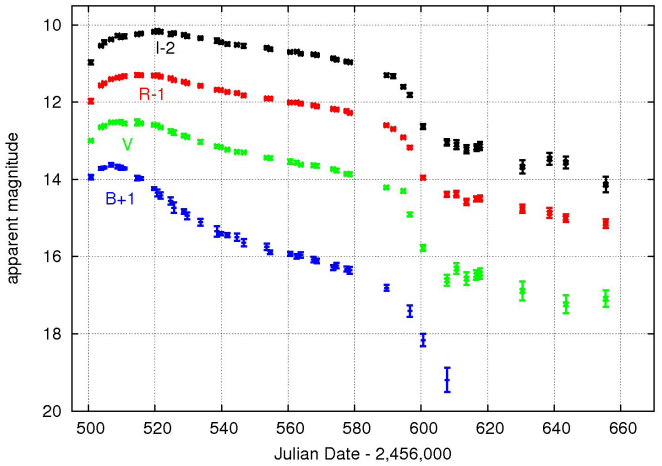

Figure 3. Light curves of SN 2013ej measured at RIT Observatory. The *B*, *R*, and *I* data have been offset vertically for clarity. No correction for extinction has been made.

Table 4. Apparent magnitudes at maximum light.

Passband	*JD–2456500*	*Magnitude*
B	7.3 ± 0.2	12.64 ± 0.01
V	12.1 ± 1.0	12.48 ± 0.02
R	14.9 ± 1.0	12.28 ± 0.01
I	19.0 ± 2.0	12.17 ± 0.02

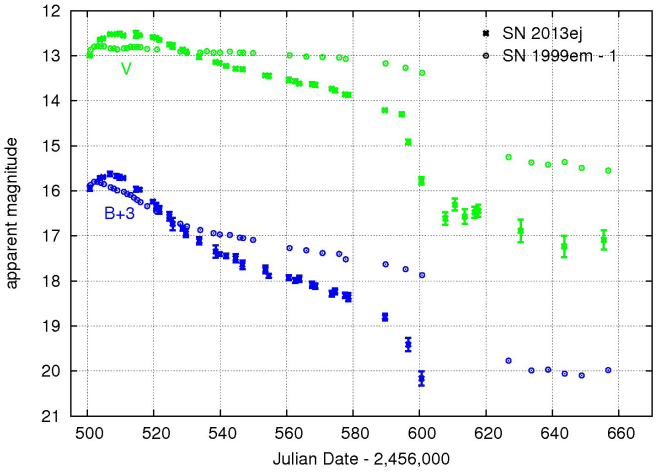

Figure 4. Light curves of SNe 2013ej and 1999em compared in the *B* and *V* passbands. The measurements of SN 1999em have been shifted horizontally (by 5,019 days) and vertically (by –1 mag.) for easier comparison.

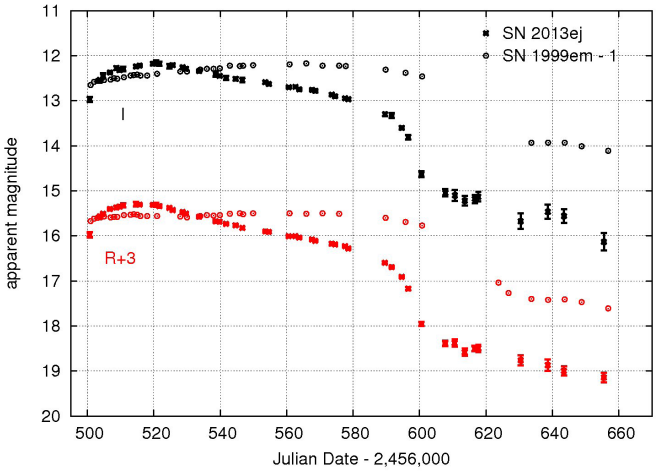

Figure 5. Light curves of SNe 2013ej and 1999em compared in the *R* and *I* passbands. The measurements of SN 1999em have been shifted horizontally (by 5,019 days) and vertically (by –1 mag.) for easier comparison.

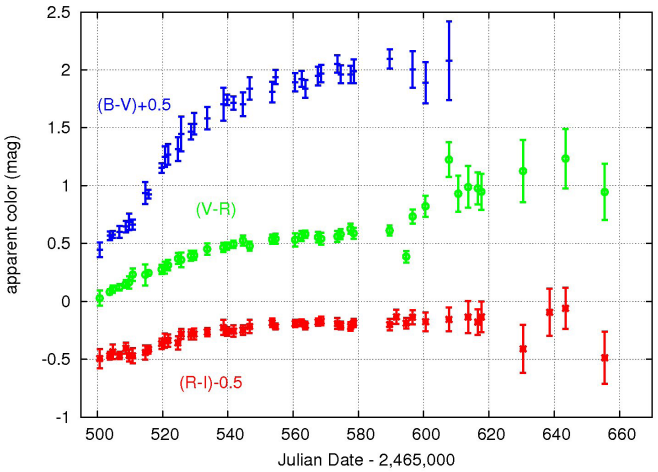

Figure 6. Color curves of SN 2013ej measured at RIT Observatory. The (*B*–*V*) and (R–I) data have been offset vertically for clarity. No correction for extinction has been made.

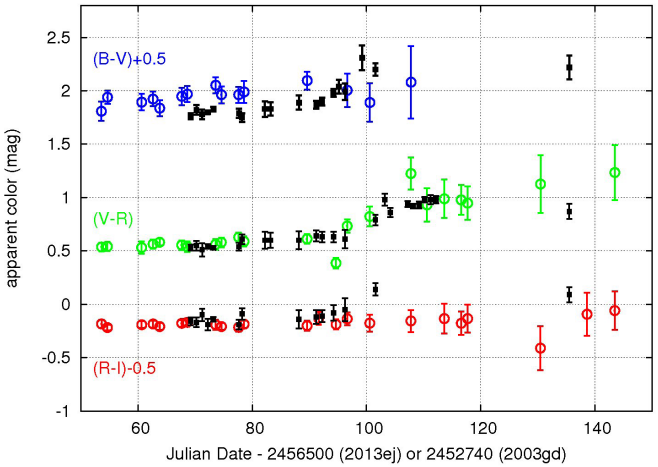

Figure 7. Color curves of SN 2013ej (large circles) compared with those of SN 2003gd (small black squares). The (B–V) and (R–I) data have been offset vertically for clarity. No correction for extinction has been made.

In order to determine the time and magnitude at peak light, I fit second- and third-order polynomials to a subset of measurements around maximum light in each passband. Table 4 lists the results. Maximum light occurs earliest in the *B*-band and successively later at longer wavelengths.

The well-observed type IIP SN 1999em (Leonard *et al.* 2002) provides a good comparison to SN 2013ej. In Figures 4 and 5, one can see that SN 2013ej rises to and falls from an early peak in all four passbands, while SN 1999em has such a peak only in *B*; its light curve is nearly flat in the other passbands. The

plateau phase ends slightly later in SN 1999em, and the drop to the late-time decline is very similar.

The colors of SN 2013ej changed considerably at the blue end of the visible spectrum, but very little at the red end. As Figure 6 indicates, the (*B–V*) color increased monotonically by about 1.5 magnitudes over one hundred days. The most rapid change occurred as the light curve fell after maximum in *B*, but the increase then slowed during the plateau phase. The (*R–I*) color, on the other hand, remained nearly constant, increasing by only 0.3 magnitude from maximum light to the plateau phase. The magnitude measurements after the end of the plateau phase are so noisy that it is hard to see any significant change in color at that time.

One can compare the colors of SN 2013ej to those of SN 2003gd, another type IIP SN in M74; this will inform the discussion of extinction in section 5. However, since SN 2003gd was discovered long after maximum light, this comparison is restricted largely to the plateau phase, and one cannot align the two events in time with any precision. Figure 7 shows the two events were very similar: SN 2003gd had a slightly smaller (*B–V*) color, but only by 0.15 magnitude at most.

5. Extinction

There are several different methods one can use to estimate the extinction along the line of sight to SN 2013ej. One can begin with the effects of dust and gas within our own galaxy: the foreground Milky Way reddening to M74 is estimated by Schlafly and Finkbeiner (2011) to be $E(B–V) = 0.062$. Note that this value is an average based on infrared maps with a beam size of order 6 arcminutes, which subtends roughly 17 kpc at the distance of M74.

In order to determine the extinction due to material within M74 itself, one might use SN 2003gd as a probe. Both it and SN 2013ej exploded within the outer southern arm of M74, the former roughly 40 degrees farther along the arm from the center of the galaxy. The similarity of the colors of these events suggests that they suffered equally from reddening. Hendry *et al.* use the colors of SN 2003gd itself, nearby stars, and nearby HII regions to derive $E(B–V) = 0.14 \pm 0.06$; this implies that the reddening contributions from M74 and the Milky Way are roughly equal.

A more direct approach is to use high-resolution spectra of SN 2013ej itself to measure the absorption lines of neutral sodium (Na I), which are correlated with extinction along the line of sight. Valenti *et al.* (2014) provide in their Figure 3 a detailed graph of the spectrum centered on the NaI D lines. As they state, this spectrum shows clearly the absorption lines due to gas within the Milky Way, but no evidence for any absorption by gas in M74. Using a digitized version of their spectrum, I measure the equivalent widths of the Milky Way components to be EW(NaI D_1) = 0.20Å and EW(NaI D_2) = 0.26Å.

The relationship in Equation 9 of Poznanski *et al.* (2012) then yields $E(B–V) = 0.049 \pm 0.010$. I will adopt this value for all following analysis.

Taking the relationships between reddening and extinction given in Schlegel *et al.* (1998) one can compute the extinction in each passband to be $A_B = 0.20 \pm 0.04$, $A_V = 0.15 \pm 0.03$, $A_R = 0.12 \pm 0.02$, and $A_I = 0.08 \pm 0.02$. If one were to choose the slightly higher reddening given by Schlafly and Finkbeiner (2011) of $E(B–V) = 0.062$, one would derive slightly larger extinctions of $A_B = 0.27 \pm 0.05$, $A_V = 0.21 \pm 0.04$, $A_R = 0.17 \pm 0.03$, and $A_I = 0.12 \pm 0.03$.

Note that the adopted reddening is roughly 0.09 magnitude smaller than that of SN 2003gd, which is consistent with the difference in the $(B–V)$ colors of the two supernovae during the plateau phase of their evolution. Both the colors of the SN 2013ej and the high-resolution spectra of Valenti *et al.* (2014) indicate that there was very little material along the line of sight within M74, and little circumstellar material surrounding the progenitor itself.

6. The distance to M74 and absolute magnitudes of SN 2013ej

In order to calculate the absolute magnitude of SN 2013ej, one must know the distance to its host galaxy. Many attempts have been made to determine this distance, using a variety of methods. The appearance of the brightest individual stars has been used to derive distance moduli of $(m – M) = 29.3$ (Sohn and Davidge 1996), 29.32 (Sharina *et al.* 1996), and 29.44 (Hendry *et al.* 2005). Sandage and Tammann (1974) measured the angular sizes of the three largest HII regions to estimate $(m – M) = 31.46$. Hendry *et al.* (2005) applied the Standardised Candle Method of Hamuy and Pinto (2002) to spectra and photometry of SN 2003gd to derive $(m – M) = 29.9^{+0.6}_{-0.7}$; they also determined a distance by assuming that SNe 2003gd and 1999em were identical, yielding $(m – M) = 30.12 \pm 0.32$. More recently, Herrmann *et al.* (2008) used the Planetary Nebula Luminosity Function (PNLF) to determine a precise value of $(m – M) = 29.67^{+0.06}_{-0.07}$. Jang and Lee (2014) kindly provided results in advance of their publication of a distance based on the Tip of the Red Giant Branch (TRGB); using HST images, they find $(m – M) = 29.91 \pm 0.04$ (rand) ± 0.12 (sys).

6.1. Applying the Expanding Photosphere Method (EPM) to SN 2013ej

The Expanding Photosphere Method (EPM) applies basic physics to determine the distance to a supernova (Kirshner and Kwan 1974; Schmidt *et al.* 1992). Using spectra or photometry, one estimates the temperature of the photosphere at a set of times; assuming that it radiates approximately as a blackbody, one can compute the luminosity per unit area. If the photosphere expands freely, then a combination of radial velocity measurements and the time since explosion permits one to compute the size of the photosphere. One can multiply these quantities to determine the luminosity of the photosphere, then compare to the observed brightness to find the distance to the event.

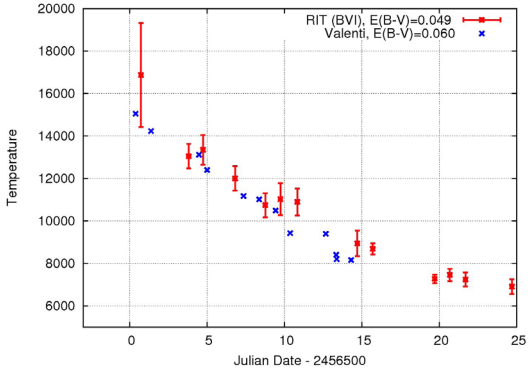

Figure 8. Temperature of SN 2013ej based on blackbody fits to *BVI* photometry from RIT, and based on *UBgVrRiI* photometry from Valenti *et al.*

Following the procedures described by Bose and Kumar (2014), I applied this technique to SN 2013ej. The temperature was calculated based on *BVI* photometry; the *R*-band values were ignored, due to the presence of strong Hα features. To estimate the uncertainties in the temperatures, I used a Monte Carlo approach: I generated thousands of instances of artificial photometric measurements by adding random gaussian noise to the actual magnitudes, then fit blackbody spectra to those artificial measurements. The temperatures derived from RIT photometry (after corrections for extinction) are shown in Figure 8; they are slightly larger than those computed by Valenti *et al.* (2014), which is somewhat surprising, since my adopted reddening is smaller than that of Valenti *et al.* (2014). However, both sets of temperatures, for the most part, do agree within the uncertainties of the RIT values. Since the RIT dataset lacks spectroscopy, I adopted the radial velocities described in Valenti *et al.* (2014), covering epochs $5 < \text{JD} - 2456500 < 22$.

The procedures of Bose and Kumar (2014) yield a semi-independent distance for each passband of photometric measurements; they are not fully independent due to the photometric color corrections, and due to the combination of magnitudes into colors which are used to determine the temperature. Plotting the time of each measurement against the ratio of angular size to photospheric velocity yields a graph in which the slope is the distance to the supernova, and the y-intercept is the time at which the size would be zero; the actual time of explosion will be somewhat later, since the star's initial size will always be larger than zero. Figure 9 shows the results of the analysis for all four passbands of RIT photometry, and Table 5 lists them.

The weighted average of these distances is $D = 9.1 \pm 0.4$ Mpc, corresponding to a distance modulus $(m - M) = 29.79 \pm 0.11$. One might conclude that the time of the explosion is roughly $t_0 \sim 2456493$, if one ignores the initial radius of the progenitor. The rise time, from explosion to maximum light, would then range

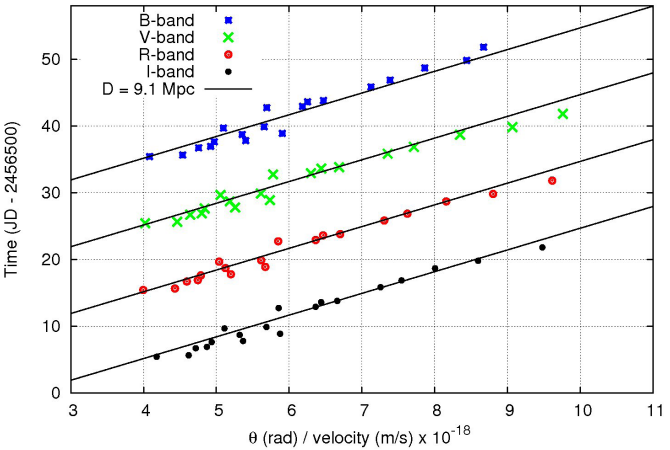

Figure 9. Distance to SN 2013ej based on EPM. The data have been shifted vertically for clarity by 30, 20, 10 days in *B*, *V*, *R*, respectively. A line corresponding to the average distance $D = 9.1$ Mpc has been drawn to guide the eye.

Table 5. Results of EPM applied to SN 2013ej.

Passband	*Distance (Mpc)*	*Time of explosion*[a]
B	10.4 ± 1.1	–9.6
V	8.5 ± 0.8	–6.4
R	8.8 ± 0.7	–6.8
I	9.4 ± 0.9	–8.2

[a]*JD–2456500; does not account for initial radius.*

from 14 days in *B* to 26 days in *I*, increasing monotonically with wavelength. This is considerably shorter than the values estimated for most of the sparsely-sampled type IIP SNe modelled by Sanders *et al.* (2014), but similar to the rise times for the well-observed type IIP SN 2012aw (Bose *et al.* 2013).

6.2. Summary of distance measurements

I give greatest weight to the PNLF (Herrmann *et al.* 2008) and TRGB (Jang and Lee 2014) methods, and so adopt a distance modulus of $(m - M) = 29.8 \pm 0.2$. Using this value, and the extinction in each passband, one can calculate the absolute magnitude of SN 2013ej at maximum light; the results are shown in Table 6.

How does this event compare to other type IIP SNe? Richardson *et al.* (2002) examine the absolute magnitudes of 29 type IIP events, finding a mean value $M_B = -17.00 \pm 1.12$. It appears that SN 2013ej falls close to the middle of this distribution, indicating that it was typical of its class.

Table 6. Absolute magnitudes at maximum light, corrected for extinction.

Passband	*Magnitude*[a]
B	–17.36 ± 0.04 ± 0.20
V	–17.47 ± 0.04 ± 0.20
R	–17.64 ± 0.02 ± 0.20
I	–17.71 ± 0.03 ± 0.20

[a]*Absolute magnitude followed by random uncertainty, then systematic uncertainty.*

7. Visual vs. CCD measurements

Because SN 2013ej was one of the closest supernovae in the past few decades, it was monitored intensively by visual observers. It provides us with a rare opportunity to compare visual measurements of a type IIP supernova to CCD *V*-band measurements.

I collected visual estimates from the AAVSO's website (AAVSO 2014). There were a total of 119 measurements, all with validation flag value "Z," indicating that they had been checked only for typos and data input errors. The visual measurements cover the period $1 < \text{JD} - 2456500 < 105$, which starts shortly before maximum light and continues to the end of the plateau phase. For each of the CCD V-band measurements, I estimated a simultaneous visual magnitude by fitting an unweighted low-order polynomial to the visual measurements within *N* days; due to the decreasing frequency of visual measurements and the less sharply changing light curve at late times, the value *N* was increased from 5 days to 8 days at JD 2456540 and again to 30 days at JD 2456565. The differences between the polynomial and each V-band measurement are shown as a function of CCD (*B*–*V*) color in Figure 10.

An unweighted linear fit to these differences yields the relationship

$$(\text{visual} - \text{V})_{2013\text{ej}} = -0.15 + (0.25 \pm 0.02) \times (B-V). \quad (6)$$

This is very similar to the relationship between visual and CCD *V*-band measurements of the type Ia SN 2011fe found by Richmond and Smith (2012):

$$(\text{visual} - \text{V})_{2011\text{fe}} = -0.09 + (0.19 \pm 0.04) \times (B-V). \quad (7)$$

The fact that two SNe of different type are perceived by human eyes in a similar fashion is consistent with the fact that their light is dominated by the continuum at these relatively early times. In fact, the degree to which eyes judge a supernova to be fainter as it grows redder agrees with the relationship for ordinary stars measured by Stanton (1999), further suggesting that human eyes are responding primarily to the continuum emission of supernovae.

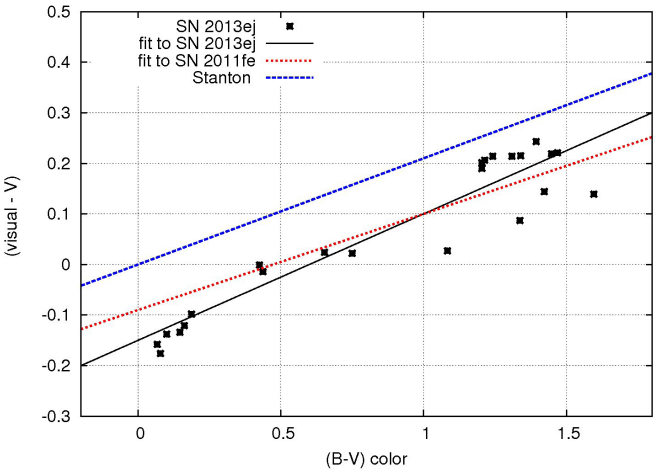

Figure 10. Difference between visual and CCD *V*-band measurements of SN 2013ej, together with relationships for SN 2011fe (Richmond ans Smith 2012) and variable stars (Stanton 1999).

8. Conclusion

Photometric *BVRI* measurements from the RIT Observatory of SN 2013ej for six months after its discovery show that it was a typical type IIP supernova. After correcting for extinction and assuming a distance modulus $(m - M) = 29.8$, I find absolute magnitudes of $M_B = -17.36$, $M_V = -17.47$, $M_R = -17.64$, and $M_I = -17.71$. Applying the expanding photosphere method to this event yields a distance modulus of $(m - M) = 29.79 \pm 0.11$, agreeing well with other recent values. The very low extinction along the line of sight, and the proximity of its host galaxy M74, make this one of the brightest core-collapse supernovae since 1993. As a result, many visual observers were able to monitor SN 2013ej for over three months; the differences between their estimates and CCD *V*–band measurements reveal the same trend with color that one sees in type Ia supernovae and in ordinary stars.

9. Acknowledgements

We thank Arne Henden and the staff at AAVSO for providing a sequence of comparison stars near M74, and the many observers who contribute their time, energy, and measurements to the AAVSO. Stefano Valenti very gently pointed out an error in the early version of this work and kindly provided temperatures based on his own photometry. Insung Jang cheerfully volunteered to choose M74 as the next target in his project to measure distances to nearby galaxies.

The anonymous referee made several suggestions which improved this paper. MWR is grateful for the continued support of the RIT Observatory by RIT and its College of Science.

References

AAVSO. 2013, observations from the AAVSO International Database (http// www.aavso.org).
Bessell, M. S. 1990, *Publ. Astron. Soc. Pacific*, **102**, 1181.
Bose, S., and Kumar, B. 2014, *Astrophys. J.*, **782**, 98.
Bose, S., *et al.* 2013, *Mon. Not. Roy. Astron. Soc.*, **433**, 1871.
Fraser, M., *et al.* 2014, *Mon. Not. Roy. Astron. Soc.*, **439**, 56.
Hamuy, M., and Pinto, P. A. 2002, *Astrophys. J.*, **566**, 63.
Hendry, M. A., *et al.* 2005, *Mon. Not. Roy. Astron. Soc.*, **359**, 906.
Herrmann, K. A., Ciardullo, R., Feldmeier, J. J., and Vinciguerra, M. 2008, *Astrophys. J.*, **683**, 630.
Honeycutt, R. K. 1992, *Publ. Astron. Soc. Pacific*, **104**, 435.
Jang, I. S., and Lee, H. M. 2014, private communication.
Kim, M., *et al.* 2013, *Cent. Bur. Astron. Telegrams,* No. 3606, 1.
Kirshner, R. P., and Kwan, J. 1974, *Astrophys. J.*, **193**, 27.
Landolt, A. U. 1992, *Astron. J.*, **104**, 340.
Leonard, D. C., *et al.* 2002, *Publ. Astron. Soc. Pacific*, **114**, 35.
Monet, D. G., *et al.* 2003, *Astron. J.*, **125**, 984.
Poznanski, D., Prochaska, J. X., and Bloom, J. S. 2012, *Mon. Not. Roy. Astron. Soc.*, **426**, 1465.
Richardson, D., Branch, D., Casebeer, D., Millard, J., Thomas, R. C., and Baron, E. 2002, *Astron. J.*, **123**, 745.
Richmond, M. W., and Smith, H. A. 2012, *J. Amer. Assoc. Var. Star Obs.*, **40**, 872.
Sandage, A., and Tammann, G. A. 1974, *Astrophys. J.*, **194**, 559.
Sanders, N. E., *et al.* 2014, arXiv 1404.2004S.
Schlafly, E. F., and Finkbeiner, D. P. 2011, *Astrophys. J.*, **737**, 103.
Schlegel, D. J., Finkbeiner, D. P., and Davis, M. 1998, *Astrophys. J., Suppl. Ser.*, **500**, 525.
Schmidt, B. P., Kirshner, R. P., and Eastman, R. G. 1992, *Astrophys. J.*, **395**, 366.
Sharina, M. E., Karachentsev, I. D., and Tikhonov, N. A. 1996, *Astron. Astrophys., Suppl. Ser.*, **119**, 499.
Sohn, Y-J., and Davidge, T. J. 1996, *Astron. J.*, **111**, 2280.
Stanton, R. H. 1999, *J. Amer. Assoc. Var. Star Obs.*, **27**, 97.
Treffers, R. R., and Richmond, M. W. 1989, *Publ. Astron. Soc. Pacific*, **101**, 725.
Valenti, S., *et al.* 2014, *Mon. Not. Roy. Astron. Soc.*, **438**, 101.